Geomechanics and Engineering, *Vol. 16, No. 1 (2018) 21-34*
DOI: https://doi.org/10.12989/gae.2018.16.1.021

Validation of 3D discrete fracture network model focusing on areal sampling methods-a case study on the powerhouse cavern of Rudbar Lorestan pumped storage power plant, Iran

Abbas Kamali Bandpey[1a], Kourush Shahriar[*1], Mostafa Sharifzadeh[2] and Parviz Marefvand[1]

[1]Department of Mining and Metallurgical Engineering, Amirkabir University of Technology, Tehran, Iran
[2]Department of Mining Engineering and Metallurgy Engineering, Western Australian School of Mines (WASM), Curtin University, Australia

(Received April 20, 2017, Revised January 23, 2018, Accepted March 7, 2018)

Abstract. Discontinuities considerably affect the mechanical and hydraulic properties of rock mass. These properties of the rock mass are influenced by the geometry of the discontinuities to a great extent. This paper aims to render an account of the geometrical parameters of several discontinuity sets related to the surrounding rock mass of Rudbar Lorestan Pumped Storage Power Plant powerhouse cavern making use of the linear and areal (circular and rectangular) sampling methods. Taking into consideration quite a large quantity of scanline and the window samplings used in this research, it was realized that the areal sampling methods are more time consuming and cost-effective than the linear methods. Having corrected the biases of the geometrical properties of the discontinuities, density (areal and volumetric) as well as the linear, areal and volumetric intensity accompanied by the other properties related to four sets of discontinuities were computed. There is an acceptable difference among the mean trace lengths measured using two linear and areal methods for the two joint sets. A 3D discrete fracture network generation code (3DFAM) has been developed to model the fracture network based on the mapped data. The code has been validated on the basis of numerous geometrical characteristics computed by use of the linear, areal sampling methods and volumetric method. Results of the linear sampling method have significant variations. So, the areal and volumetric methods are more efficient than the linear method and they are more appropriate for validation of 3D DFN (Discrete Fracture Network) codes.

Keywords: discontinuity; geometrical characteristics; areal sampling; 3DDFN code; validation

1. Introduction

The discontinuities in the rock mass play an important role in the connectivity, REV (representative elementary volume), deformability, permeability, strength, stress-strain relation and failure of the rock mass (Zimmerman and Main 2004, Li *et al.* 2017, Ni *et al.* 2017). Hence, in addition to the mechanical characteristics of the discontinuities and the intact rock, the characterization and representation of the geometrical parameters of discontinuities is very important when studying the behavior of the rock mass and resolving the interaction between the rock mass and structures. Fig. 1 depicts a schematic view of the key geometrical properties of discontinuities. P_{10}, P_{21} and P_{32} are defined as the number of fractures in the length unit of the Scanline, the fracture trace length divided by the sampling area unit and the fracture area divided by the rock mass volume unit, respectively. Density includes P_{20} and P_{30} are defined as the number of fracture centers in the area of the sampling zone and in the unit of the rock mass volume, respectively.

In view of the fact that the rock mass structure cannot directly be studied in three dimensions, the fracture characteristics are normally studied by use of the areal or Scanline sampling. This paper describes the geometrical parameters of 1035 discontinuities (639 fractures with Scanline and 396 fractures with areal sampling) related to the rock mass at two domains existing around the powerhouse cavern of Rudbar Lorestan Pumped Storage Power Plant project located in Iran measured based on the linear and areal (circular and rectangular) sampling methods. The discontinuities were sufficiently mapped in the underground spaces and include 1035 joints, which are considered well above the required minimum limit (i.e. 100 for each set) (Kulatilake *et al.* 1993).

The cavern under consideration is located in the extensional zone of an anticline. The study area is highly fractured due to being located in High Zagros Zone affected by the recent Orogeny. Therefore, the first step in modeling the geometry of the joints existing in the rock mass is to explore the homogenous statistic areas in this domain (Kulatilake *et al.* 1990). The discontinuities have been surveyed at different locations. Hence, equality of two and multi mean and variance test (ANOVA) (Pallat 2004) have been resorted to in controlling the homogeneity of the data and studying the relatively uniform rock mass domain. Several methods have been developed to correct the sampling biases allowing for the uncertainty in the mapped data (Kulatilake and Wu 1984, Zhang and Einstein 1998).

*Corresponding author, Professor
E-mail: K.shahriar@aut.ac.ir
[a]Ph.D. Student
E-mail: abbas.kamali@aut.ac.ir

http://www.techno-press.org/?journal=gae&subpage=7 ISSN: 2005-307X (Print), 2092-6219 (Online)

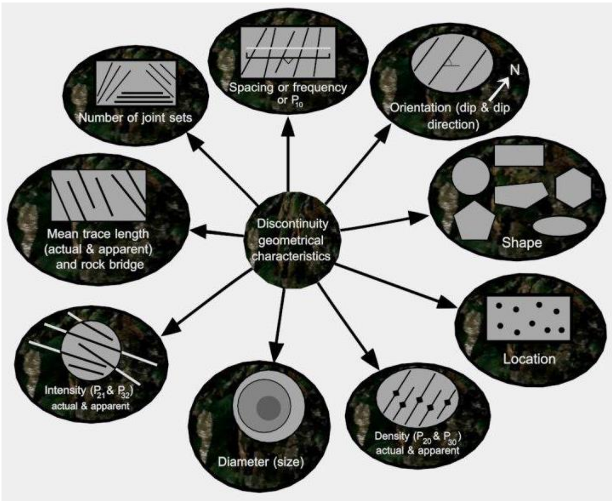

Fig. 1 Schematic view of the geometrical characteristics of the discontinuities

The correction of biases of the mapped data is necessary for the upcoming assessments. In addition, in order to validate the DFN models, it is essential to make use of the unbiased data.

It is very difficult to measure the entire properties of the discontinuities in 3 dimensions due to the fact that the discontinuities are buried in the rock mass (Zheng *et al.* 2014). For this reason, DFN models can be very advantageous in view of producing different realizations out of the fracture network as for recognizing the 3D geometrical behavior of the discontinuities. There have been developed several methods for generating the DFN models (Xu and Dowd 2010, Reeves *et al.* 2013, Zhang and Yin 2014). In this research, the discrete fracture network generation code, 3DFAM(3 Dimension of Fracture Characterization Analysis using Mapping Methods) has been developed on 3D basis using Matlab Software.

Taking into consideration the great significance of the specifications of the Fisher's constant as well as the values of intensity (linear, areal and volumetric) and the density (areal and volumetric) in generating and validating the 3DFAM (Mauldon *et al.* 1999a, Zhang and Einstein 2000, Rohrbaugh *et al*. 2002), they have been computed for each set of discontinuity. The definition of intensity and density of discontinuities is presented in section 4.4 and 4.5, respectively. The volumetric intensity of the discontinuities is considered as the very important specifications for generating the DFN models. So, these values were computed for the joint sets and the bedding under consideration applying two different methods.

It is very important to validate the DFN models in which it is very challenging due to the complexity. The previous studies have mostly used the linear intensity (Scanline method) to validate the DFN model (Kulatilake *et al*. 1993, Xu and Dowd 2010, Noroozi *et al*. 2015). There has also been used some specifications as the dip, dip direction, Fisher's coefficient, trace length making use of the rectangular window (Kulatilake *et al*. 1993, Xu and Dowd 2010) and the trace length making use of the circular window sampling (Zhang and Ding 2010) for one or two joint sets. The DFN Models have rarely been validate on the basis of the linear, areal and volumetric intensity of three joint sets surveyed in the tunnel using circular and rectangular window sampling. These joint sets have different dip and dip direction and low k-Fisher constant. Because the larger amount of k-Fisher depicts less scattered fractures. Hence, in this research, the mean trace length based on the areal method, areal intensity, volumetric intensity and the areal density of the joint sets around the powerhouse cavern has been utilized in addition to the parameters of dip, dip direction, linear intensity and Fisher's coefficient to validate the 3DFAM code.

2. Geological condition and field mapping

Rudbar Lorestan Pumped Storage Power Plant with the hydropower generation capacity of 1000 MW is being constructed in about 100 km south of the city of Aligoodarz in Lorestan Province of Iran. In accordance with the structural - sedimentary classification of Nabavi (1976), Rudbar Lorestan Pumped Storage Power Plant is located in the structural - sedimentary zone of High and tectonized Zagros. In regional scale, the bedrock of this zone includes the rocks of the primary to tertiary geological eras. The powerhouse cavern area has been constituted by Dalan Formation consisting of moderate to thick bedded limestone and dark gray dolomitic limestone.

The scanline, circular or rectangular sampling methods are used to record the geometrical characteristics of the discontinuities in the rock outcrops. The method of Scanline is widely used. It provides a quick analysis on the fractures characteristics. In this method, the fracture density cannot be computed, but it is possible to determine the linear intensity (Zeeb *et al.* 2013). This method is affected by the biases of orientation, size, cutting and censoring (Priest 1993). The orientation of the fracture proportionate to the scanline is the reason for the presence of the foregoing biases. The areal sampling results in 2D data of the fracture network such as the density and the areal intensity (Zeeb *et al.* 2013). However window sampling have all biases and may also has bias for size measurement e.g. due to truncation and censoring effects and 2D observation of 3D systems. There is disadvantage in both linear and areal mapping methods; they map only the exposed surface.

Sampling methods of scanline and areal including the circular, rectangular and square windows have been resorted to for studying and estimating the geometrical and mechanical characteristics of the discontinuities existing around the powerhouse cavern. But the geometrical characteristics of discontinuities have been analyzed. According to Fig. 2, there has been excavated a 120 m long horseshoe-section tunnel with dimensions of 6 m * 6 m as an exploratory gallery in the crown of the powerhouse cavern. In addition, there has also been excavated a 514 m long horseshoe-section grouting gallery with dimensions of 3 m * 4m (w * h) in 25 m away from the powerhouse cavern axis and 20 m above the crown of the powerhouse cavern. The powerhouse cavern is being excavated in an approximate depth of 400 m with dimensions of 49.5 m * 26.3 m * 129.75 m (height * width * length).

Eleven scanlines with lengths ranging between 10 m and 16 m have been used so as to survey the discontinuities of

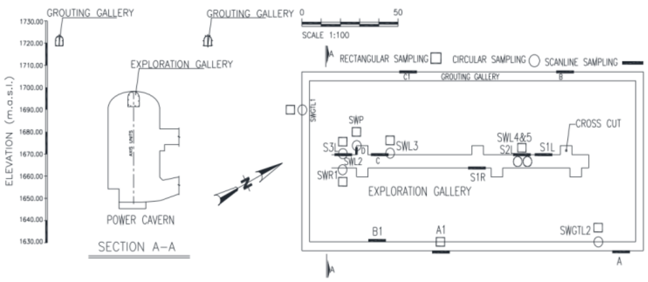

Fig. 2 Location of the exploratory tunnel in the crown of the powerhouse cavern, peripheral grouting gallery accompanied by the scanlines (thick lines) and areal samplings

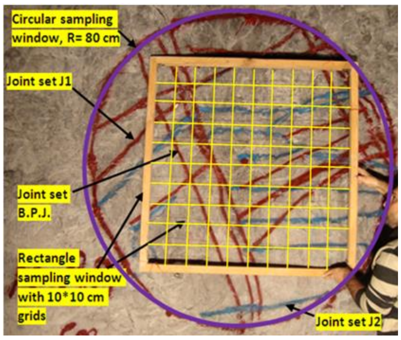

(a)

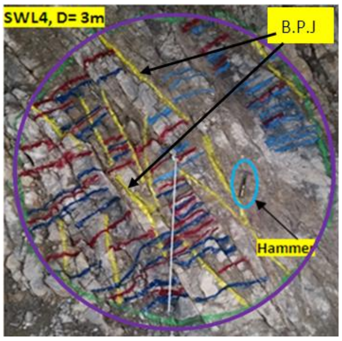

(b)

Fig. 3 (a) Circular window sampling with radius of 80 cm (SWL4) accompanied by square method (1*1m with 10*10 cm grids) and (b) diameter of 3 m (SWL3) in exploratory tunnel in the crown of the powerhouse cavern

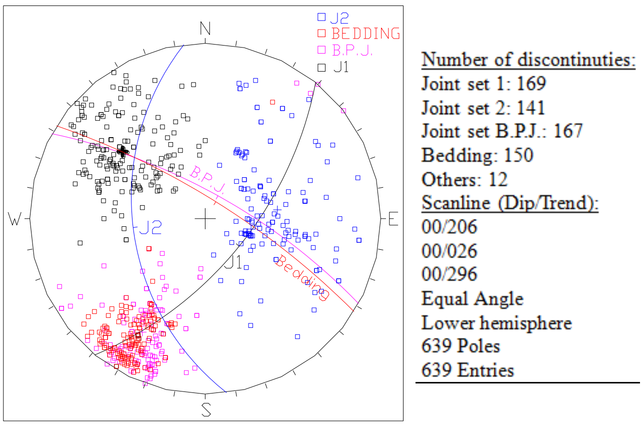

Fig. 4 All discontinuities poles mapped accompanied by the number of discontinuities in each set and direction of the scanlines.

the aforementioned locations, Fig. 2. For all joint sets, the length of the scanline is 20 to 32 times of the mean spacing. In some locations of exploratory gallery, the trends of scanlines are perpendicular together to survey of discontinuities characteristics in two directions. In accordance with Fig. 2 eleven circular windows sampling with radius of 55 cm to 1.5 m and 15 rectangular window samplings with dimensions of maximum 2.2 m*1.9 m have been used as well. Figs. 3(a) and 3(b) depict circular window sampling with radius of 80 cm (SWL3). As item 3, two tests were conducted on the data and they show the homogeneity of the mapped data. So, all scanline surveys and areal samplings reveal the same DFN model statistics and they can be combined.

In all mappings, efforts have been made to consider the general recommendation pertaining to the survey of 130 to 350 joints in each sampling zone that 50% of them have at least one visible end (Priest 1993). In this study, 1035 discontinuities have been mapped. The poles of the foregoing discontinuities (639 surveyed fractures with scanline method) accompanied by the specifications of the scanlines have been presented in Fig. 4. The third joint set is of Bedding Plane Joint (B.P.J.) type (as the strike joint set) allowing for the geometrical location of the joint set proportionate to the bedding. The B.P.J.is somehow parallel and they have very close distance to bedding, but their length is very less than bedding, Fig. 3. Note that, only scanline method has been used in the study area as for the bedding and discontinuity of B.P.J. which are longer than 16 m and 2 m respectively. Nevertheless, the B.P.J. characteristics have been studied in one circular window and two rectangular windows.

3. Study on the homogeneity of the mapped data

Taking into consideration the discontinuities mapped in two separate locations, it is necessary to perform the required assessments on the statistical homogeneity of the characteristics of the discontinuities and determine the unit rock mass domain. So, two tests were conducted on the data of dip, dip direction and spacing.

3.1 Test of comparing the variance and mean of two populations

In order to study of the equality of two means tests, it is necessary to see whether the variance of the two populations is equal or not. In other words, the variance equality test takes priority over the mean equality test. Levene test (Pallat 2004) is used for the variance equality test. In Levene test, it is not needed to have normal distribution of data. Besides, the Levene test can be used when the number of samples is not the same. The statistic of Levene test is F (Fisher). The statistic of t for the mean equality test of two grouping variables (populations) as independent variables (Pallat 2004) is computed in two cases of the equality and non-equality test of the variance of two grouping variables under consideration. The two grouping variables are the grouting gallery and the exploratory tunnel located in the powerhouse cavern crown

Table 1 Results of the equality mean and variance test of the grouting gallery and the exploratory tunnel (two grouping variables) located in the powerhouse cavern crown

Type of discontinuity	(Levene Test) H0: σ2CT= σ2GG			(t Test) H0: μCT=μGG		
	Dip	Dip Direction	Spacing	Dip	Dip Direction	Spacing
Bedding	Ok	Ok	Ok	Ok	Ok	Ok
J1	No	Ok	No	Ok	Ok	Ok
J2	No	Ok	Ok	No	Ok	Ok
B.P.J.	Ok	Ok	Ok	Ok	Ok	Ok

CT is Cavern roof Tunnel, GG is Grouting Gallery

Table 2 Results of Analysis of Variance (ANOVA) test for the left and right walls in the grouting gallery and the exploratory tunnel located in the powerhouse cavern crown

Type of discontinuity	H0: μCTR= μCTL = μGGR =μGGL		
	Spacing	Dip Direction	Dip
Bedding	Ok	Ok	Ok
J1	CTR is not homogenous	Ok	Ok
J2	Ok	Ok	GGR & GGL are not homogenous
B.P.J.	Ok	Ok	Ok

CTL is Cavern roof Tunnel, Left wall, CTR is Cavern roof Tunnel, Right wall, GGL is Grouting Gallery, Left wall, GGR is Grouting Gallery, Right wall, Ok denotes all subsets (CTL, CTR and GGL& GGR) are located in same set and they are homogeneous

and the test variables (as dependent variables) include the dip, dip direction and spacing. The results of the mean and variance equality test of two grouping variables at a 5% significance level are presented in Table 1. In all cases in which the null hypothesis has been rejected in t test, the mean value of the grouting gallery is more than the mean value of the grouping variable of the exploratory tunnel. As seen, the null hypothesis is acceptable for the variables of dip direction and spacing related to the whole set of discontinuities. The reason why null hypothesis not accepted for the variable of the dip in one case of J2 is the low Fisher’s constant that will be explained in the sub-item 4-1.

3.2 Analysis of variance (ANOVA) of several populations

This analysis is used to compare the mean of two or several grouping variables (i.e., the effect of an independent grouping variable on a dependent list variable). The analysis of variance that is called ANOVA can be also constructed for a regression analysis (Yoon *et al*. 2015). The statistic of this test is F. In this case, the left and right walls of the grouting gallery and the exploratory tunnel are the independent grouping variables and the dependent list variables are the dip, dip direction and spacing. The test of Tukey has been used so as to study on the significant differences two by two among different groups. A significance level of 5% has been considered for the test. As seen in Table 2, the joint sets are homogeneous in regard to the dip direction and spacing. When the quantitative dependent variable is the dip, the reason for the non-homogeneity of some joint sets is the low Fisher’s constant that will be explained in the sub-item 4-1.Table 2 indicates that data are homogenous in four locations.

In accordance with the given tests, it can be assumed that there is homogeneity among the data of two grouping variables (the grouting gallery and the exploratory tunnel). It is notable that it is necessary to study the homogeneity of the mapped characteristics so as to validate the DFN models due to the selection of the homogeneous Poison’s technique in DFN code.

4. Geometrical characteristics of discontinuities

4.1 Orientation of Discontinuities

Orientation includes dip and dip direction. It is a parameter by which the discontinuity plane can be determined in space. There are 4 sets of discontinuities (three joint sets plus bedding). It is necessary to have some corrections taking into consideration the orientation bias encountered while mapping the discontinuities. The orientation data including the dip and dip direction has been corrected (omission of bias) (Priest 1993). The final results have been presented in Table 3. The angle of ρ is the angle between the scanline and the Fisher’s mean pole which is required for converting the linear and areal intensity to the volumetric intensity (Wang 2005). In this assessment, the orientation of all discontinuities under consideration has been modeled making use of the Fisher's distribution. The Fisher’s constant is generally in the range of 5 to 440 (Kemeny and Post 2003, Baghbanan 2008). In accordance with Table 3, except for the bedding, other discontinuities have a Fisher's constant of less than 20. This indicates that the highly tectonized of the area under consideration and the fact that the cavern is located in close proximity to main fault.

4.2 Termination of discontinuities

The situation of the discontinuities at the end is called termination. So, the records of the nature and the termination conditions of the discontinuities semi-trace length are very important (Brown 1981, Priest 1993). The index of termination in order to quantify the amount of termination parameter is given by (Priest 1993) as Eq. (1).

$$T_i = \frac{100\ N_i}{N_i + N_a + N_o}\% \qquad (1)$$

where, N_i, N_a and N_o are the number of discontinuities that their semi-trace has terminated in intact rock, abutted to another discontinuity and become hidden respectively. The termination status of each discontinuity was recorded while mapping the 639 discontinuities. Table 4 represents the measured values of N_i, N_a, N_o and calculated T_i related to each joint set. As presented in Table 4, most of the joints are of restricted fracture type and the termination index of the rock mass is less than 5%. As presented in the classification of ISRM (1981), the rock mass of the cavern,

Table 3 Corrected dip and dip direction values together with the Fisher's constant and ρ angle values

Type	Dip (°)		Dip Direction (°)		K-Fisher		ρ angle (°)	
	Uncorrected	Corrected	Uncorrected	Corrected	Uncorrected	Corrected	Along 00/206 & 01/026 (D. /D.D.)	Along 001/296
Bedding	77	76	032	033	28.6	25.6	15.6	*
J1	62	60	129	123	13.5	17.3	84	30
J2	45	46	263	280	6.6	9.5	78.6	47
B.P.J.	73	70	029	029	11	10.4	20.2	*

D.: Dip, D.D.: Dip Direction

Table 4 Number of semi traces in terms of the type of termination and the index of termination based on the type of joint sets

Type	Ni	Na	No	Ti (%)
Bedding	1	21	278	0.4
J1	4	288	46	1.2
J2	2	242	38	0.7
B.P.J.	9	247	78	2.7

with regard to the T_i value, is described as sub-systematic and/ or closely jointed rock mass.

4.3 Persistence of discontinuities

4.3.1 Trace length of discontinuity in scanline method

Scanline is one of the most conventional methods applied in recording the discontinuity data. With regard to the finite size of the surveying area, there are some biases of censoring and truncation at the time of mapping. For this reason, it is necessary to correct the length biases (Priest and Hudson 1981).

So as to eliminate the curtailment bias, a cut off length of minimum 5 cm has been taken into consideration. With regard to the type of the probable density function and the curtailment level (Priest 1993), the method of ncr has been used to correct the bias of discontinuities. In this method, n, c and r are total number of discontinuities, curtailment level and number of discontinuities that their semi trace length is less than c, respectively (Priest 1993, Priest and Hudson 1981). The curtailment level computed for the J1, J2 and B.P.J. is equal to 200 cm, 230 cm and 400 cm respectively. Given the above, the weight mean amount and the weight standard deviation computed for the trace length of the discontinuities of J1, J2 and B.P.J. are equal to 64 and 53 cm, 68 and 54 cm, 219 and 108 cm respectively. In accordance with the ISRM classification, the J1 and J2 are of very low persistence type and the B.P.J. is of low persistence type (Brown 1981).

With regard to the assessment results and field investigations carried out at the site exposed area, the bedding persistence in 80% and 20% of the mapped data are in the range of 10 m to 20 m (high persistency (Brown 1981)) and more than 20 m (very high persistency (Brown 1981)) respectively. So, in accordance with the data measured in the field (more than 70 layers) and field observations, the mean and standard deviation of the bedding trace length were calculated equal to 16 m and 4 m respectively.

Goodness of fit (GOF) tests of Kolmogorov-Smirnov, Anderson-Darling, and Chi-Square in a 5% significant level have been used to select the best Probability Distribution Function (PDF) of discontinuity set trace length . Besides, value of test statistic, P value and P-P plot have been used to rank PDFs. So, the trace length of the joint sets J1 and J2, follow the lognormal distribution. But, the distributions of Weibull and uniform are suitable for B.P.J. joint set.

In this study, circular shape (equidimensional) has been assumed as the geometry of discontinuities. Meanwhile, the trace length and the diameter follow the same distribution function. With regard to mean value, standard deviation and the type of the trace length PDF computed for 4 sets of discontinuity, the values of mean and standard deviation of Bedding, J1, J2 and B.P.J. diameter are 21 and 2.8 m, 0.58 and 0.28 m, 0.72 and 0.33 m, 2.73 and 0.4 m, respectively.

4.3.2 Trace length of discontinuity in circular and rectangular window sampling methods

Window sampling method is also applied to measure the discontinuity. As opposed to the scanline method, the window sampling is an areal method which let more discontinuity data be collected. Sometimes line sampling can also collect enough data based on a larger domain. It is required to have 10 circular windows with a diameter larger than the block size and the spacing, but much smaller than the dimensions of the sampling area so as to compute the mean trace length of the fracture (Rohrbaugh *et al*. 2002). As presented in Table 5, the equations and estimators presented by the researchers have been used so as to calculate the mean trace length applying linear and areal sampling methods. In Table 5, the letter M. refers to method number.

In accordance with the results of the window sampling technique, the mean trace length of the J1 and J2 is in the range of 26 cm (method 2) to 67 cm (method 5) and 37 cm (method 2) to 100 cm (method 5) respectively. Applying different methods, the average of the results of all windows related to the J1 and J2 was computed and compared with the values obtained from the scanline method in Fig. 5. In Fig. 5, the methods with numbers 6, 7, 8 and 9 are average of methods 3, 4 and 5, methods 3 and 4, methods 3 and 5, methods 4 and 5, respectively. In view of the difference in the biases of the trace length and censoring in the linear and areal methods, the computed mean length of the traces of the two methods is different.

Making use of the areal methods (average of total mapping windows with some methods), the mean trace length of the J1, J2 and B.P.J. was calculated as 47, 68 and 125 cm, respectively. The assessment results indicate that the method presented by Laslett (1982) (Eq. (10)) is not so suitable for trace length calculation. In addition, it seems that the trace length is overestimated to some extent by use of equations 8. So, all methods have not been used in final computation of the joint sets mean trace length. The standard deviation values of the J1, J2 and B.P.J. in the areal method using the equation presented by Zhang and Ding (2010) are 13 cm, 21 cm and 34 cm respectively. Taking into consideration the results of the two linear and areal

Table 5 Fractures trace length evaluation methods (Priest 1993, Mauldon 1998, Mauldon *et al.* 1999a, Zhang and Einstein 2000)

Remarks	Formula	Equation number	Type of sampling
Average line (apparent)	$l_m = \frac{\sum l_i}{N}$	2	Scanline sampling
Pahl (Log-normal), (M. 10)	$l_m = \frac{l(h-2\eta)(N+N_O-N_2)}{(l\cos\emptyset + h\sin\emptyset)(N-N_O+N_2)}$	3	Rectangle sampling
Pahl (Exponential), (M. 11)	$l_m = \frac{l(h-\eta)(N+N_O-N_2)}{(l\cos\emptyset + h\sin\emptyset)(N-N_O+N_2)}$	4	
Average square (apparent), (M. 12)	$l_m = \frac{\sum l_i}{N}$	5	
Mauldon and Zhang (M. & Z.), (M. 1)	$l_m = \frac{\pi(N+N_0-N_2)}{2(N-N_0+N_2)}c$	6	Circular sampling
Andersson and Devrstrop, (A.&D.No. 1), (M. 3)	$l_m = \frac{2l_{tot}}{N-N_0+N_2}$	7	
Andersson and Devrstrop, (A.&D.No. 2), (M. 4)	$l_m = \frac{l_{tot}}{N-N_0}$	8	
Andersson and Devrstrop, (A.&D. No. 3), (M. 5)	$l_m = \frac{\pi c l_{tot}}{\pi c N - 2l_{tot}}$	9	
Laslett, (M. 2)	$l_m = \frac{\sum x_i + \sum y_i + \sum z_i}{2N_2 + N_1}$	10	
Average circle (apparent), (M. 13)	$l_m = \frac{\sum l_i}{N}$	11	

N is total number of fractures, N_0 is number of fractures with two ends censored (two ends are invisible), N_2 is number of fractures with two visible ends, N_1 is number of fractures with one visible end, x_i is trace length with two visible ends, y_i is trace length with one end censored, z_i is trace length with two ends censored, L_{tot} is total visible fracture length in the window sampling, c is window sampling radius, l_i is fracture length, l_m is mean fracture length, l and h are width and height of the window sampling, $\emptyset$ is the angle between the vertical side of the window sampling and trace length, η is cut off length

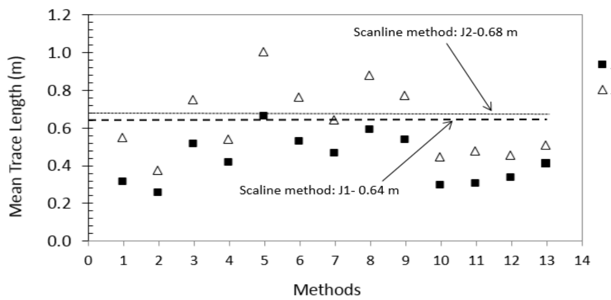

Fig. 5 Mean trace length computed using window sampling method for the J1 and J2 together with the values obtained by use of scanline method

methods, the mean trace length for the J1, J2 and B.P.J. was computed equal to 56 cm, 68 cm and 219 cm respectively. The standard deviation values for the J1, J2 and B.P.J. trace length are equal to 33 cm, 38 cm and 71 cm respectively allowing for the average of the two linear and areal methods.

Table 6 Linear Intensity values (1/m) related to each joint set in M.N.V. directions and along the scanline

Type	Set spacing (Along Scanline)		Normal (Along M.N.V.)	
	P.D.F.	P10 (1/m)	P.D.F.	P10 (1/m)
Bedding	Lognormal	1.9	Lognormal	2
J1	Weibull	1.7	Weibull	6
J2	Weibull	1.7	Weibull	4.5
B.P.J.	Lognormal	2.0	Lognormal	2.2

Table 7 Equations used for calculating the fracture intensity (Zhang and Einstein 2000, Mauldon *et al.* 2001, Rohrbaugh *et al.* 2002)

Remarks	Formula	Equation number	Type of sampling Method
Frequency	$P_{10} = {}^1/_S$	13	Scanline sampling
-	$\frac{N}{L}$	14	
Apparent intensity	$\frac{\sum x_i + \sum y_i + \sum z_i}{l * h}$	15	Rectangle sampling
Apparent intensity	$\frac{l_{tot}}{\pi c^2}$	16	Circular sampling
Mauldon's estimator	$\frac{N+N_O-N_2}{4*c}$	17	

P_{10} is linear intensity, S is spacing between the fractures, L is length of scanline, and the rest parameters are similar to Table 5

4.4 Intensity of discontinuities

The frequency or intensity of the discontinuity is one of the fundamental measurements in resolving the degree of the rock blockiness in one direction (Priest 1993). There are three types of intensities including linear (P_{10}), areal (P_{21}) and volumetric (P_{32}) that all of them have L^{-1}dimension, L is length. So, taking into account the significance of this issue, the three kinds of intensities have been considered for the discontinuities of the study area.

4.4.1 Linear intensity of the joint sets and total frequency

The linear intensity is defined as the number of fractures in the length unit of the scanline (Eqs. (13) and (14) in Table 7). The frequency or the linear intensity (P_{10}) is one of the most important parameters applied to calibrate the discrete fracture network model. The values of linear intensity related to each joint set along scanline (set spacing) and Mean Normal Vector (M.N.V.) directions of the scanline have been presented in Table 6. The total frequency value, λ_s, of 4 sets of discontinuities along the scanline (N26E) is equal to 4 (1/m) making use of the Eq. (12) by Priest (1993) as Eq. (12).

$$\lambda_s = \sum_{i=1}^{D} \lambda_i \cos \delta_i (-90^\circ \le \delta_1 \le 90^\circ) \tag{12}$$

D is the total number of the discontinuity sets, λ_i is frequency in normal direction of ith discontinuity set and δ_i is the acute angle between the sampling line and the normal vector of the discontinuity set.

4.4.2 Areal intensity

The areal intensity is defined as the fracture trace length divided by the sampling area unit (Rohrbaugh *et al*. 2002). The Eq. (17) (Zhang and Einstein 2000, Mauldon *et al*. 2001) in Table 7 has been used to calculate the areal intensity (P_{21}) by use of the circular window (as actual intensity) and the Eqs. (15) and (16) have been used in Table 7 to calculate the apparent intensity using rectangular and circular windows. The average value of the actual and apparent intensities using rectangular and circular windows of all window samplings related to the J1 are equal to 3, 3.6 and 3.4 (1/m) and the ones related to the J2 are equal to 3.7, 4.8 and 4.3 (1/m) respectively. According to the window sampling (SWL4) results, the areal intensity of the B.P.J is equal to 1.8 (1/m).

4.4.3 Volumetric intensity

P_{32} is defined as the fracture area divided by the rock mass volume unit (Dershowitz and Herda 1992). In this study, the volumetric intensity of the joint sets is calculated based on two methods of Kulatilake *et al*. (1993) and Zhang and Einstein (2000).

Zhang and Einstein proposed the equation to calculate the P_{32} of rock mass as Eq. (18) (Zhang and Einstein 2000).

$$P_{32} = \frac{N_T E(A)}{V} \tag{18}$$

where N_T is the total number of sampled discontinuities, $E(A)$ is the mean discontinuity area calculated with Eq.19 and V is the unit volume (here considered $1m^3$).

$$E(A) = \int_0^\infty \frac{\pi}{4} E(D)^2 g(D) dD = \frac{\pi}{4}[E(D)^2 + V(D)] \tag{19}$$

where $E(D)$ is mean diameter and $V(D)$ is variance of diameter.

In the method of Zhang and Einstein, it is required to calculate the number of the sampled discontinuities in the unit of volume. So, a window with dimensions of 1 * 1 m and grids of 10 * 10 cm was constructed as illustrated in Fig. 3(a).

Kulatilake *et al.* proposed the equation to calculate the P_{32} of rock mass as Eqs. (20) and (21) (Kulatilake *et al*. 1993).

$$P_{32} = \lambda_v E(A) \tag{20}$$

$$\lambda_v = P_{30} = \frac{4\lambda_m}{\pi E(D^2) E(|n.i|)} \tag{21}$$

where λ_v (P_{30}) is 3-D density of discontinuities, λ_m is the one-dimensional intensity along the mean normal vector of the discontinuity set and is equal to the reciprocal of the mean trace spacing along the mean normal vector of the discontinuity set, E(.) is the expected value of the function within the parentheses, $E(D^2)$ can be estimated based on the diameter (D) distribution, n is the unit normal vector of individual discontinuity from the discontinuity set, i is the mean unit normal vector of the discontinuity set.

In the method of Kulatilake *et al*., P_{32} calculation requires having the volumetric density. The spacing of the joint in 2 dimensions is used so as to calculate the spacing of the joint in 3 dimensions (Zhang *et al*. 2013). Hence, linear intensity along the M.N.V. has been utilized to compute the volumetric density. The volumetric intensity of all discontinuities applying Kulatilake *et al.* method and the average of the window samplings results with Zhang and Einstein method for the J1 and J2 have been presented in Table 8.

Table 8 Volumetric intensity (1/m) of all discontinuities (applying Kulatilake et al. method) and the average of the results of the window sampling (applying Zhang and Einstein method) for the J1 and J2

Type	Kulatilake *et al.* method	Zhang and Einstein method
Bedding	1.8	*
J_1	6.2	3.8
J_2	5.0	5.4
B.P.J.	2.3	*

As seen in Table 8, the error of P_{32} calculated by the foregoing two methods for the J1 and J2 is 38% and 7% respectively. This shows that it is difficult to estimate such a characteristic in the field which is led to uncertainty. In view of the fact that the shape of discontinuities has been assumed as a circular disk and the centers of the disks follow the homogeneous Poison's distribution, in order to simulate the fractures in DFN model the results of the of Kulatilake et al. method were taken into consideration (Kulatilake *et al*. 1993).

4.5 Density of discontinuities

Density includes three kinds of linear (P_{10}), areal or trace density (P_{20}) and volumetric (P_{30}) defined as the number of fracture centers in the unit of length, area of the sampling zone and the unit of the rock mass volume respectively. The units of the above characteristics are L^{-1}, L^{-2} and L^{-3} respectively. The estimation of this parameter is affected by censoring and the length bias (Dershowitz and Herda 1992, Mauldon *et al*. 1999a, 2001). In order to compute P_{20} (it is supposed as an actual density), Table 9 represents the Eqs. (23) and (25) for the discontinuity sets of J1 and J2 with circular and rectangular windows (Mauldon *et al*. 1999a, 2001). The average of the actual density values of the circular and rectangular windows as well as the apparent density for both window samplings related to the J1 are equal to 7.5, 7.8, 9.1 and 11.2 ($1/m^2$) respectively and for J2 are equal to 6.2, 6.9, 8.7 and 11 ($1/m^2$) respectively. In accordance with the obtained results, the actual densities of the J1 and J2 are 7.7 and 6.5 ($1/m^2$) respectively.

5. Three dimension DFNE code development and its application for rock mass cavern

5.1 Construction of 3D model of cavern fractures of Rudbar Lorestan

Three-dimensional DFNE code (3DFAM) has been

Table 9 Equations used for computing the fracture trace density (Mauldon *et al.* 1999a, 2001)

Remarks	Formula	Equation number	Type of sampling method
Apparent density	$\frac{N_1+N_2+N_0}{l*h}$	22	Rectangle sampling
Mauldon's estimator	$P_{20}=\frac{2N_2+N_1}{2*l*h}$	23	
Apparent density	$\frac{N_1+N_2+N_0}{\pi c^2}$	24	Circular sampling
Mauldon's estimator	$\frac{N-N_0+N_2}{2\pi c^2}$	25	

P_{20} is areal density, the other parameters are similar to Table 5

Table 10 Number of fractures generated based on the joint set and realization number using 3DFAM Code

Type Discontinuity	Number of discontinuity generated at each realization				
	1	2	3	4	5
Bedding	20	18	18	26	20
J1	51891	50253	51423	51451	51501
J2	26767	26601	26796	26830	26720
B.P.J.	703	686	675	685	690

developed in MATLAB software. In this code, the joint geometry is represented by a stochastic model because ideally each joint geometry parameter is characterized statically. The calculation procedure of 3DFAM code is illustrated in Fig. 6. The followings aspects of rock mass could be investigated using 3DFAM code.

-Calculation of the parameters existing in the equations 1 to 11, 13 to 17 and 22 to 25 (such as N_0,N_1,N_2,N_{total}, l_{tot}, etc.)

-The effect of the shape and size of window sampling

-Three types of surveying methods including scanline, circular and rectangle sampling windows and the possibility of drilling the boreholes to determine the mean trace length, intensity and density of the fracture trace in 1, 2 and 3 dimensions (actual and apparent)

-Computation of the discontinuities connection and other issues

In 3DFAMcode, the fractures center has been defined based on Baecher's disk and developed Fisher's model and the number of fractures has been generated using homogenous and stochastic Poison's process (Xu and Dowd 2010) and a uniform distribution has been used to simulate the fractures location (Zheng *et al*. 2015). The workflow of the 3D DFNE program from the beginning of the fracture generation to the validation stage of the code is illustrated in Fig. 6. Making use of the 3DFAM code, it would be possible to model 5 joint sets together with random fractures and fault (unlimited number) as a 3D circular disk. The geometrical characteristics of the joints can be defined non-deterministically. In these calculations, it has been assumed that there is no pattern heterogeneity in modeling. The output can be presented in both graphical and digitized format using the developed code. The digitized output comprises the coordinates of the center and the number of fractures, values of P_{32} ‹P_{30} ‹P_{20} ‹P_{21}, size of the trace length of the fractures after creating unlimited sections in arbitrary orientation, apparent and actual density and intensity, RQD, etc.

The data obtained in previous sections have been used for constructing the 3D Model of the fractures of Rudbar Lorestan Cavern and the fractures have been generated in a block with dimensions of$12*12*12\ \mathrm{m}^3$. The simulation includes 5 realizations of the fracture network and the average of the parameters under consideration has been applied in the calculations. The number of the fractures generated in each realization has been given in Table 10. Six circular and rectangular (same area with the circle) window samplings with the same center and 6 scanlines with a length of 11 m (each one) at a suitable location (at heights 1, 3, 6, 7, 9 and 11 m in section plane) have been used to record the required data from generated fractures. The radii of the circular window samplings are 0.6, 1, 1.4, 1.7, 2 and 3 m. For instance, in a case study, circular windows with radii of 1 to 2 m have been utilized in the open surfaces and fractures with the lengths ranging between 0.4 m and 1.65 m (Weiss 2008).

Dimensions of the windows have been selected taking into consideration the real conditions encountered in the tunnels and slopes. The size of the rock block relies upon the spacing or the fracture frequency. So, this issue is considered as a problem for estimators as to the mapping window smaller than the block size, and effects on the estimation of the fracture parameters (Rohrbaugh *et al*. 2002). Therefore, it is necessary to have at least 10 circular surveying window with a radius larger than the fracture spacing or the block size, but much smaller than the dimensions of the study area. Besides, it is necessary to sample over 30 fracture end points in each window sampling (Rohrbaugh *et al*. 2002, Zeeb *et al*. 2013). These are reasons why the window sampling has been enlarged.

Having created the 3D block of the discrete fracture network, as set out in Fig. 7, it would be possible to create sections with any direction or even inclined (with arbitrary dip and dip direction) in arbitrary location. With regard to the larger diameter of the bedding than the other joint sets and for better illustration, the bedding disks have not been shown in Fig. 7. Bedding plane is formed by sedimentary process (rather than mechanical breakage) so, it thus may not be appropriate to represent it using disk. Of course, the validation of DFN code has been done with considering of three joint sets.

The direction of the inclined section in use is 85/116 (dip/dip direction) taking into consideration the discontinuity data mapping direction in the exploratory tunnel and around the powerhouse cavern. In other words, the sampling planes in DFN model follow the plane of sampling that they used for surveys. It passes through the middle of the block as shown in Figs. 7 and 8. The reason why the circular window has been shown in elliptic shape is the rotation of the section in x-z direction. So, in accordance with the created 2D sections, the geometrical characteristics of the joint sets (actual and apparent) are calculated in three sampling methods based on the Eqs. (1)-(11), (13)-(17) and (22)-(25) for each 4 sets separately.

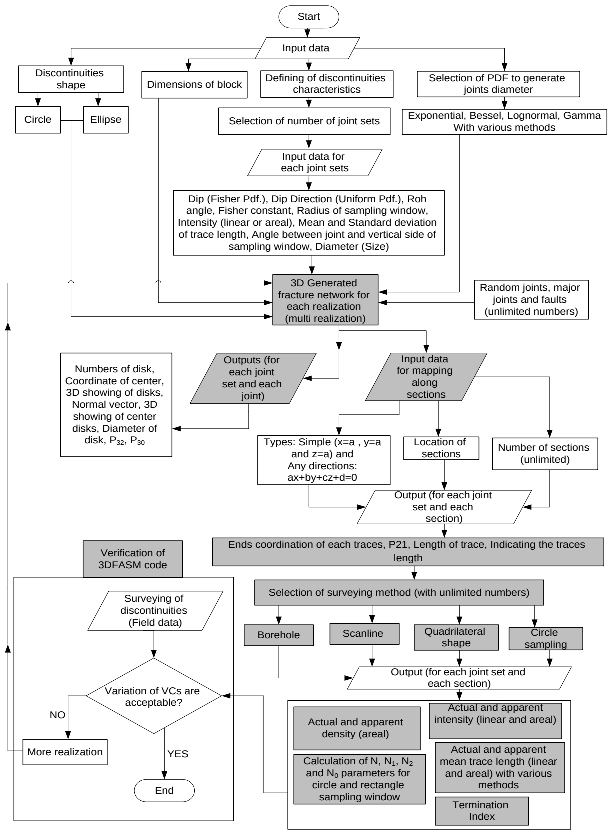

Fig. 6 Workflow of developed DFN code, 3DFAM

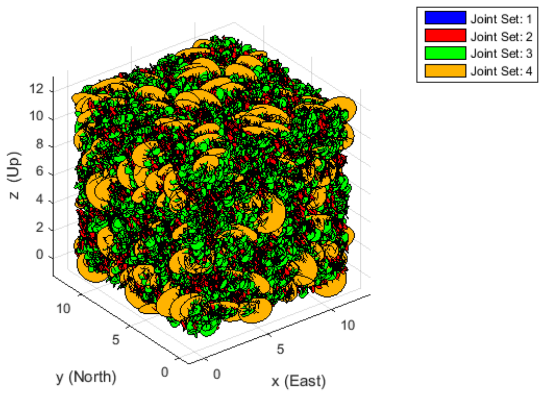

(a)

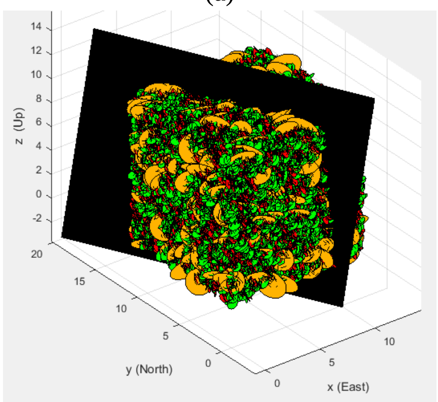

(b)

Fig. 7 (a) 3D generated fracture network (4 joint sets) of the cavern rock mass together with (b) the inclined section in 85/116 direction

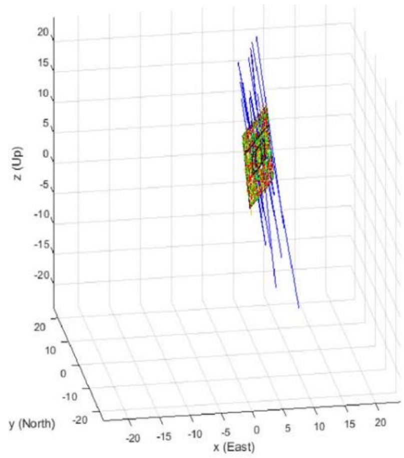

(a)

(b)

Fig. 8 (a) 3D inclined section, orientation 85/116 and (b) the three sampling methods (scanline, circular and rectangular sampling) in the section under consideration, x-z direction

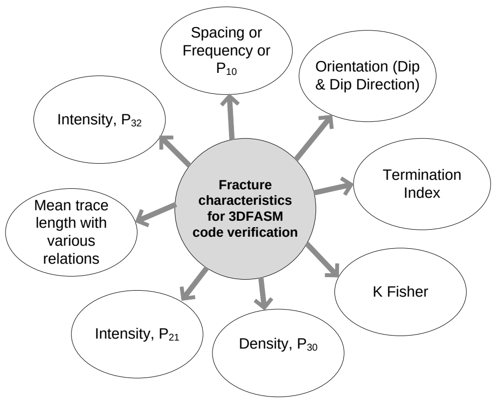

Fig. 9 Geometrical characteristics of the discontinuity used for validating the 3DFAM code

5.2 Validation of the fracture network model and discussion

Taking into consideration the calculation of the whole geometrical characteristics of the joint sets as the input

Table 11 Linear intensity RD values calculated using 3DFAM code with the measurement value (%) and its maximum difference amongst the realizations

Joint set	Realization number					Maximum difference between realizations (%)
	1	2	3	4	5	
J_1	16.6	0.5	23	13	15	98
J_2	13	4.3	17.5	6.4	10	75
B.P.J.	23	27	28	30	25	23
Bedding	8.5	26	32	9.4	20	71
Total sets	38	32	24	36	33	37

Table 12 Deviation percentage of the linear intensity value calculated making use of 3DFAM code between the scanline in 6 m and 7 m position

Joint set	Realization number	Difference (%)
J_2	1	31
B.P.J.		38
J_2	2	35
B.P.J.		40
J_1	3	34
J_1	4	50
J_2		50
Total sets		34

Table 13 Intensity RD value calculated using 3DFAM code with the measurement value

Method	P_{10} (1/cm)				
	J1	J2	B.P.J.	Bedding	Total sets
Code	0.0158	0.0185	0.0145	0.0158	0.058
Field data	0.017	0.017	0.02	0.019	0.04
RD	7%	8.8%	27.5%	16.8%	45%

Table 14 Trace length RD values calculated using 3DFAM code with its measurement value

Method	Trace length (cm)		
	J_1	J_2	B.P.J.
Field data	56	68	219
Code, Eq. (6)	56	59	192
RD	0%	13%	12%
Code, Eq. (2)	51	62	186
RD	9%	9%	15%
Code, Average of Eqs. (7) & (9)	43	60	196
RD	23%	12%	10%
Code, Eq. (3)	41	55	198
RD	26%	19%	9.6%

parameter of 3DFAM code and the generation of the 3D fracture network of powerhouse cavern, the validation of this code is the most significant stage according to the aforesaid data. In this assessment, so as to validate the generated fracture network, the parameters of trace length (using estimators and different equations), areal intensity, volumetric intensity, areal density and termination index by use of circular and rectangular sampling have been resorted to apart from the common geometrical properties such as the linear intensity, dip, dip direction and Fisher's coefficient. Fig. 9 depicts the geometrical characteristics of the discontinuity utilized for validating the 3DFAM code.

The areal sampling method was focused on account of its high efficiency compared with the linear method and the fact that all existing data are analyzed on the surface. In this study, absolute magnitude of Relative Difference Percentage (RD%) has been considered equal to the percentage of the difference between the mean of field data and computed value as a result of the code divided by the field data as the acceptance criteria. Provided that RD is less than 30%, it can be said that the field data and the code output comply with each other (Kulatilake *et al*. 1993). However, in the homogeneous fracture pattern, a 15% error is acceptable for the actual intensity value (Rohrbaugh *et al*. 2002).

Although it is possible to calculate the intensity quickly making use of the scanline method, this method has biases such as orientation, length, censoring and pattern heterogeneity (the fracture pattern is not homogenous). In accordance with the numerical assessment done, in view of the orientation bias, decrease in the dip angle of the joint set from 60 to 10 degrees, the difference between P_{10} and P_{21} would increase from 10 to 80% (Kamali *et al*. 2016). Due to the orientation bias, when the scanline or the longitudinal axis of the sampling area is not perpendicular to the joint set, the estimated intensity value is lower (Rohrbaugh *et al*. 2002). Besides, in this method, the measured trace length is inaccurate, because the scanline preferably intersects the larger trace lengths and it is not possible to completely measure traces length on the rock surface with restricted size (Priest and Hudson 1981). One of the weakness points of the scanline method in validating the generated fracture network model is the considerable variation of the linear intensity value allowing for the change in the position of the scanline in the model. Table 11 represents the RD values of the linear intensity computed using the code with the value measured for each realization. Each figure presented in Table 11 is the average of 6 scanlines.

As seen in Table 11, there are considerable variations in the RD of the joint sets mostly. In addition, their difference between the realizations for most of the joint sets is more than 70%. In accordance with the assessments done, sometimes one meter of displacement of the scanline has given rise to major variations in the results. Table 12 represents only the linear intensity difference in the 6 m and 7 m scanlines which have 30% to 50% variations in some realizations and for some joint sets. It shows that the amount of P_{10} of each joint set is very sensitive to Scanline location. Table 13 represents the RD of the linear intensity computed using the 3DFAM code with its amount measured in the study area. As seen in the results, the variations of RD are so considerable with regard to the dislocation of the scanline. However, there is an acceptable compatibility between the linear intensity values measured in the study area and the values computed using the 3DFAM code. It

Table 15 Dip, dip direction and Fisher's coefficient calculated using 3DFAM code with their measurement values

Characterization	Method	Type of discontinuities			
		Bedding	J_1	J_2	B.P.J.
Dip	Field data	76	60	46	70
	Code	77	61	49	65
Dip Direction	Field data	33	123	280	29
	Code	34	128	289	34
K-Fisher	Field data	25.6	17.3	9.5	10.4
	Code	28.7	19.4	10.5	12

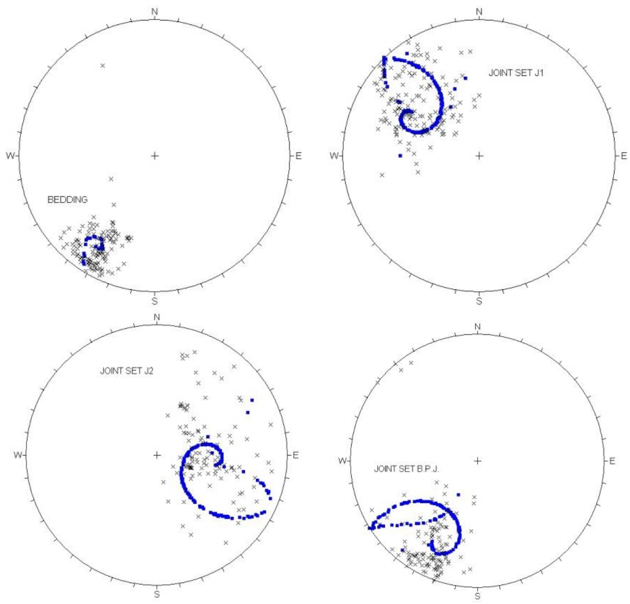

Fig. 10 Stereographic image of a number of fractures simulated using 3DFAM code along with the whole mapped fractures in the study region based on each joint set

shows that the 3DFAM code for evaluating and studying of linear intensity is suitable. But, average of more than 5 scanlines should be used to calculate the linear intensity and for comparing with field data.

The equations presented in Table 5 have been used to study the difference between the trace length computed by use of the code and measured in the study area. The numerical assessment results have indicated that the Eqs. (3), (6), (7) and (9) (presented in Table 5) are appropriate for computing the mean trace length and are not affected by the biases of the length and censoring (Kamali *et al*. 2016). In other words, the mean trace length of the fractures has been computed not only by the linear method (Eq. (2)), but also by the areal method. As seen in Table 14, the RD value for each joint set has always been less than 15%. Eq. (8) shows no suitable mean trace length value as to the three joint sets of J1, J2 and B.P.J.. In other words, the difference between this equation and mean trace length value of the study region are 37%, 32% and 49% respectively, for the three foregoing joint sets. The difference of more than 25% of this equation with the actual trace length value based on the numerical analysis carried out for 4 synthetic joint sets

Table 16 RD values for the areal and volumetric intensity and areal density calculated using 3DFAM code with the measurement values

Method	P_{32} (1/m)		
	J_1	J_2	B.P.J.
Code	6.9	5.7	1.5
Field data	6.2	5	2.3
RD	11%	14%	35%
	P_{30} (1/m^3)		
Code	29.7	15.5	0.39
	P_{21}		
Code (population)	3.4	4.2	1.4
Code, Eq. (17)	3.8	4.0	1.5
Field data	3	3.7	1.8
RD (with code, population)	13%	13%	22%
RD (with Code, Eq. (17))	26%	8%	17%
	P_{20} (1/m^2)		
Code (population)	8.1	7.6	0.82
Code, Eq. (25)	7.0	7.4	0.80
Code, Eq. (23)	8.2	8.4	0.84
Field data	7.7	6.5	-
RD (with code, population)	5%	17%	-
RD (with Code, Eq. (25))	9%	14%	-
Difference (with Code, Eq. (23))	6%	29%	-

has also been approved (Kamali *et al*. 2016).

Table 15 represents the dip, dip direction and Fisher's coefficient calculated by use of the code and their measurement values. As seen, the RD value of the characteristics set forth for all joint sets is less than 15%. Fig. 10 depicts the stereographic image of a number of the simulated fractures of the whole joint sets (20 beddings and for other joint sets, 200 fractures for each joint set) together with all fractures mapped in the study area. The blue points in Fig. 10 are the simulated fractures with 3DFAM code and the cross markers are mapped fractures in the field. As seen, there is a reasonable compliance between the measured orientation values of the study area and the ones generated by use of the code.

Making use of some characteristics such as the areal and volumetric intensity and areal density, it would be possible to study the fracture behavior in three and two dimensions and commensurate with the dimensions of the window sampling, more fractures can be studied. So, the aforementioned characteristics have also been utilized by use of the circular and rectangular sampling methods so as to have a more accurate validation over the fracture network generation code. To this end, the Eqs. (17), (23) and (25) as well as the values of P_{32} ‹P_{21} and P_{20} generated using 3DFAM code have been resorted to as the population values of the generated fracture. As seen in Table 16, in most cases, RD values for the three joint sets is less than 30%. For all joint sets, due to the censoring effects, the apparent density values are more than the population density. The apparent density depends on the scale as a result of the edge

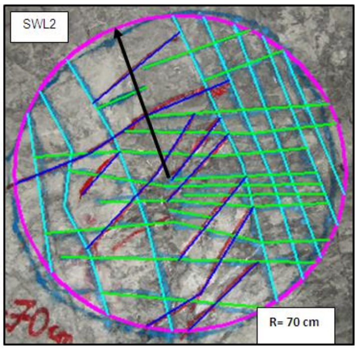

(a)

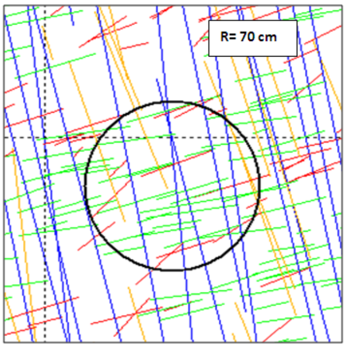

(b)

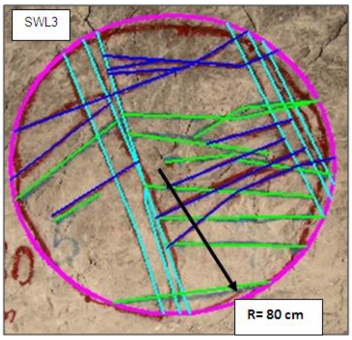

(c)

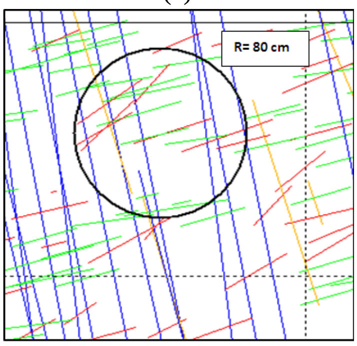

(d)

Fig. 11 Comparison between predicted and field observed fracture traces on sampling window: (a) trace of four joint sets obtained from mapping on the sampling window SWL2; (b) predicted fracture traces of four joint sets on sampling window; (c) trace of four joint sets obtained from mapping on the sampling window SWL3; (d) predicted fracture traces of four joint sets on sampling window. In field sampling windows of SWL2 and SWL3: Cyan traces: Bedding and B.P.J., Blue traces: J1 and Green traces: J2. In predicted fracture traces: Blue traces: Bedding, Red traces: J1, Green traces: J2 and Buff traces: B.P.J

effects (Dershowitz and Herda 1992, Mauldon *et al.* 1999b). Whilst, the estimators presented by Mauldon *et al.* (2001), Eqs. (23) and (25), do not depend on the scale and the censoring and length biases are corrected automatically. Hence, the equations under consideration are suitable for validating the DFN code.

Normally, in the 2D sections passing through the 3D block of the fracture network generated by use of DFN codes, the fractures cross each other even with a short length; so, the N_i value increases and the calculated termination index value increases accordingly proportionate to the actual conditions as well. As stated in Item 4-2, the cavern surrounding rock is of closely jointed type, but on the basis of the termination index values computed using the code, the rock mass is of moderately jointed type. Therefore, in this study, numerous simulations indicated that the termination index is not an appropriate criterion for validating the 3DFAM code.

To support the validation and comparison, map of joint traces sampled from DFN model and field survey on the sampling windows SWL2 and SWL3 are presented in Fig. 11(a), 11(b) and Fig. 11(c), 11(d). To support the validation and comparison, map of joint traces sampled from DFN model are compared with field survey in Fig. 11. According to Figs. 11(a) and 11(b) as well as Figs. 11(c) and 11(d) compare quite well with respect to statistical properties of fracture traces.

Accordingly, with regard to the performed one, two and three dimensional assessments, there is a reasonable compliance between the measured data and the characteristics of the generated fractures. So, the 3DFAM code is reliable enough for.

6. Conclusions

In this paper, the following 5 points can be concluded in accordance with the results of 1035 discontinuities mapped by use of linear and areal sampling methods in the cavern surrounding tunnels, computation of the geometrical characteristics of the discontinuity sets together with the correction of all biases, generation and development of the discrete fracture network code (3DFAM) and the validation of this code based on the actual data:

1- The geometrical characteristics measured and calculated using two linear and areal methods (e.g. mean trace length of the joint sets) should not normally have a difference of more than 30%. So, it is required to make use of a scanline with different lengths and window sampling with various dimensions and diameters (commensurate with the discontinuity trace length).

2- The Orogeny and high tectonized area of the region under study, the presence of active faults, being located in the anticline tensile zone and the map of the discontinuities at two locations have given rise to the performance of the equality of two and multi means and variance test (ANOVA) for studying the homogeneity of the data. Since the code of 3DFAM has been developed on the basis of the homogeneous Poison's process, it is necessary to review the homogeneity of the mapped data for validating the code. In other words, doing of some tests on geometrical parameter to evaluate the homogeneity of the data are necessary.

3- The differences in the mean trace length computed between two linear and areal methods for the J1, J2 and B.P.J are 26, 0 and 43% respectively. This difference is acceptable for the J1, but it is better to have a window sampling diameter of about 4 m taking into consideration the low Fisher's constant and the trace length of the B.P.J that is larger than 2 m. It is notable that the window sampling with a diameter of 4 m is not so easy allowing for the tunnel dimensions and the way to get access. Furthermore, there have been recognized more appropriate equations and estimators for calculating the mean trace length.

4- It is very difficult to compute the volumetric intensity of the discontinuities in the study area and as presented in the obtained results, the difference between the volumetric intensity of the discontinuities in the foregoing methods for the J1 and J2 is 38% and 7% respectively. It is necessary to determine the volumetric intensity for validating the DFN Models.

5- In order to validate the 3DFAM code, some characteristics as the trace length (making use of the different estimators and equations), areal and volumetric intensity and the areal density by use of the circular and rectangular sampling methods have also been utilized apart from the use of the linear sampling method. The RD value computed for the areal intensity is also less than 20%; it has been less than 15-30% for the other characteristics in most cases. The linear and areal assessments indicate that there is a reasonable compliance between the measured data (mapped data) and the characteristics of the fracture generated using the developed code and the code of 3DFAM is reliable enough. In other words, several characteristics were calculated to validate the model. As shown in section 5-2, the most of RD values are low.

Acknowledgements

We herewith appreciate the technical, executive and financial supports of the companies Iran Water & Power resources Development Co. (IWPC), Mahab Consulting Engineering Co., Hara, Taban and Falord Companies (Project contractors) collaborated in mapping the discontinuities existing around the powerhouse cavern.

References

Baghbanan, A. (2008), “Scale and stress effects on hydro-mechanical properties of fractured rock masses”, Ph.D. Dissertation, KTH Royal Institute of Technology, Stockholm, Sweden.

Brown, E.T. (1981), *ISRM Suggested Methods: Rock Characterization, Testing and Monitoring*, Pergamon Press, London, U.K.

Dershowitz, S.D. and Herda, H.H. (1992), “Interpretation of fracture spacing and intensity”, *Proceedings of the 33rd US Symposium on Rock Mechanics*, Santa Fe, New Mexico, U.S.A., June.

Kamali, A., Shahriar, K., Sharifzadeh, M., Aalianvari, A. and Esmaeilzadeh, A. (2016), “Effect of shape and size of window sampling on the determination of average length, intensity and density of trace discontinuity”, *Proceedings of the Symposium on the Rock Mechanics and Rock Engineering*, Cappadocia, Turkey, August.

Kemeny, J. and Post, R. (2003), “Estimating three-dimensional rock discontinuity orientation from digital images of fracture traces”, *Comput. Geosci.*, **29**(1), 65-77.

Kulatilake, P.H.S.W. and Wu, T.H. (1984), “Estimation of mean trace length of discontinuities”, *Rock Mech. Rock Eng.*, **17**(4), 215-232.

Kulatilake, P.H.S.W., Wathugala, D.N. and Stephansson, O. (1993), “Joint network modeling with a validation exercise in Stripa Mine, Sweden”, *J. Rock Mech. Min. Sci. Geomech. Abstr.*, **30**(5), 503-526.

Kulatilake, P.H.S.W., Wathugala, D.N. Poulton, M. and Stephansson, O., (1990), “Analysis of structural homogeneity of rock masses”, *J. Eng. Geol.*, **29**(3), 195-211.

Li, Y., Chen, J. and Shang, Y. (2017), “Connectivity of three-dimensional fracture networks: A case study from a dam site in southwest China”, *Rock Mech. Rock Eng.*, **50**(1), 241-249.

Mauldon, M, Rohrbaugh Jr., M.B., Dunne, W.M. and Lawdermilk, W. (1999), “Mean fracture trace length and density estimators using circular windows”, *Proceedings of the 37th U.S. Symposium on Rock Mechanics (USRMS)*, Vail, Colorado, U.S.A., June.

Mauldon, M. (1998), “Estimating mean fracture Trace length and density from observations in convex window”, *J Rock Mech. Rock Eng.*, **31**(4), 201-216.

Mauldon, M., Dunne W.M. and Rohrbaugh Jr., M.B. (2001), “Circular scanline and circular windows: New tools for characterizing the geometry of fracture traces”, *J. Struct. Geol.*, **23**(2-3), 247-258.

Mauldon, M., Rohrbaugh Jr., M.B., Dunne, W.M. and Lawdermilk, W. (1999), “Fracture intensity estimates using circular scanlines”, *Proceedings of the 37th U.S. Symposium on Rock Mechanics (USRMS)*, Vail, Colorado, U.S.A., June.

Ni, P., Wang, S., Wang, C. and Zhang, S. (2017), “Estimation of REV size for fractured rock mass based on damage coefficient”, *Rock Mech. Rock Eng.*, **50**(3), 555-570.

Noroozi, M., Kakaie, R. and Jalali, S.E. (2015), “3D geometrical-stochastical modeling of rock mass joint networks: Case study of the right bank of Rudbar Lorestan Dam plant”, *J. Geol. Min. Res.*, **7**(1), 1-10.

Pallat, J. (2004), *SPSS Survival Manual*, Amazon Publisher Inc.

Priest, S.D. (1993), *Discontinuity Analysis for Rock Engineering*, Chapman and Hall Press, London, U.K.

Priest, S.D. and Hudson, J.A. (1981), “Estimation of discontinuity spacing and trace length using scanline surveys”, *J. Rock Mech. Min. Sci. Geomech. Abstr.*, **18**(3), 183-197.

Reeves, D.M., Parashar, R., Pohll, G., Carroll, R., Badger, T. and Willoughby, K. (2013), “The use of discrete facture network simulations in the design of horizontal hillslope drainage networks in fractured rock”, *J. Eng. Geol.*, **163**, 132-143.

Rohrbaugh Jr., M.B., Dunne, W.M. and Mauldon, M. (2002), “Estimating fracture trace intensity, density and mean length using circular scanlines and windows”, *AAPG Bull.*, **86**(12), 2089-2104.

Wang, X. (2005), “Stereological interpretation of rock fracture traces on borehole walls and other cylindrical surfaces”, Ph.D. Dissertation, Virginia Polytechnic Institute and State University, Blacksburg, Virginia, U.S.A.

Weiss, M. (2008), “Techniques for estimating fracture size: A comparison of methods, Technical note”, *J. Rock Mech. Min. Sci.*, **3**(45), 460-466.

Xu, C. and Dowd, P. (2010), “A new computer code for discrete fracture network modeling”, *Comput. Geosci.*, **36**(3), 292-301.

Yoon, S., Lee, S.R., Kim, Y.T. and Go, G.H. (2015), “Estimation of saturated hydraulic conductivity of Korean weathered granite soils using a regression analysis", *Geomech. Eng.*, **9**(1), 101-113

Zeeb, C., Gomez-Rivas, E., Bons, P.D., Virgo, S. and Blum, P. (2013), "Fracture network evaluation program (FraNEP): A software for analyzing 2D fracture trace-line maps", *J. Comput. Geosci.*, **60**, 11-22.

Zhang, L. and Ding, X. (2010), "Variance of non-parametric rock fracture mean trace length estimator", *J. Rock Mech. Min. Sci.*, **7**(47), 1222-1228.

Zhang, L. and Einstein, H.H. (1998), "Estimating the mean trace length of rock discontinuities", *Rock Mech. Rock Eng.*, **31**(4), 217-235.

Zhang, L. and Einstein, H.H. (2000), "Estimating the intensity of rock discontinuities", *J. Rock Mech. Min. Sci.*, **37**(5), 819-837.

Zhang, Q.H. and Yin, J.M. (2014), "Solution of two key issues in arbitrary three-dimensional discrete fracture network flow models", *J. Hydrol.*, **514**, 281-296.

Zhang, W., Chen, J., Cao, Z. and Wang, R. (2013), "Size effect of RQD and generalized representative volume elements: A case study on an underground excavation in Baihetan dam, Southwest China", *Tunn. Undergr. Sp. Technol.*, **35**, 89-98.

Zheng, J., Deng, J., Yang, X., Wei, J. Zheng, H. and Cui, Y. (2014), "An improved Monte Carlo simulation method for discontinuity orientations based on Fisher distribution and its program implementation", *J. Comput. Geotech.*, **61**, 266-276.

Zheng, J., Deng, J., Zhang, G. and Yang, X. (2015), "Validation of Mont Carlo simulation for discontinuity locations in space", *J. Comput. Geotech.*, **67**, 103-109.

Zimmerman, R.W. and Main, I. (2004), *Hydromechanical Behavior of Fractured Rocks*, in *Mechanics of Fluid-saturated Rocks*, Elsevier, 363-421.

GC